

Autocatalysis due to combinatorial enhancement

Nanako Hirano^{1,*}, Akira Yoshida^{1,2,†}, Takenobu Nakamura^{3,‡} and Naoko Nakagawa^{1,§}

¹*Department of Physics, Ibaraki University, Mito 310-8512, Japan*

²*Department of Physics, Kyoto University, Kyoto 606-8502, Japan and*

³*National Institute of Advanced Industrial Science and Technology (AIST), Tsukuba 305-8568, Japan*

(Dated: March 19, 2025)

We demonstrate that autocatalytic reactions, where a product catalyzes its own formation, can be significantly accelerated when the product molecules are indistinguishable from each other. This “combinatorial enhancement,” analogous to the driving force of osmotic pressure, arises from the increased multiplicity of microscopic configurations. We quantify this effect with a free-energy gain, F_{gain} , and validate our theoretical predictions using molecular dynamics simulations. We also propose an experiment to directly test this phenomenon, potentially providing new insights into self-assembly, biomolecular binding, and other cooperative processes.

Introduction: Biological systems rely on intricate networks of interacting reactions, where the product of one reaction can influence the rate of subsequent reactions. This is exemplified by cooperative binding phenomena, such as the binding of O₂ to hemoglobin [1], antibody-antigen interactions [2], and allosteric regulation of enzymes [3–6], as well as by autocatalytic processes crucial for metabolism and signal transduction [7, 8]. While numerous studies have validated binding cooperativity and developed macroscopic mathematical formalisms, the microscopic origin of this cooperativity even in single, diffusive molecules remains an open question. Traditionally, allosteric effects, attributed to the intricate structure of biomolecules, have been invoked. In this Letter, we propose a distinct mechanism for promoting binding reactions, focusing on how the concentration of reaction products enhances the rate of subsequent binding events without specifying particular materials or quantum processes. We term this phenomenon autocatalysis due to combinatorial enhancement.

Reaction rates can vary significantly depending on conditions, and often described by free energy differences along reaction coordinates, as in the Arrhenius equation, transition state theory, and Kramers’ rate theory [9–12]. Crucially, this difference is between the initial and intermediate states, not the initial and final states. Thus, identifying rate-limiting intermediate states has been central to chemical reaction studies. This is, in essence, a question of how large fluctuations are achieved. Recent advances in stochastic thermodynamics [13–19] allow us to treat feedback controls as thermodynamic operations [20]. Feedback control demonstrates that information can be a resource for engines [21–23], and provides a framework for quantifying irreversibility via fluctuation theorems [24–27]. Anomalous irreversible dynamics have been linked to large fluctuations and subsequent reaction events [28–30]. This Letter aims to formu-

late cooperative binding using these concepts of feedback control and stochastic thermodynamics.

Setup: We consider a mixture comprising n_A molecules of species A and n_B molecules of species B. A and B exhibit attractive interactions at short range, characterized by a length σ_{AB} , while interactions between identical molecules (A–A or B–B) are repulsive. Choosing constant temperature and constant volume (T, V), the combination of attractive and repulsive forces leads to temporary trapping of B around A upon collision. This process can be viewed as a reversible reaction:



resulting in the formation of a molecular complex AB₂.

Hereafter, we use indices $i \in [1, n_A]$ and $j \in [1, n_B]$ to refer to molecules of type A and B, respectively. Given $\Gamma_A \equiv (\mathbf{r}_i^A, \mathbf{p}_i^A)_{i \in [1, n_A]}$ and $\Gamma_B \equiv (\mathbf{r}_j^B, \mathbf{p}_j^B)_{j \in [1, n_B]}$, the classical Hamiltonian for the mixture is defined as

$$H_0(\Gamma_A, \Gamma_B) = \sum_{i=1}^{n_A} \frac{|\mathbf{p}_i^A|^2}{2m_A} + \sum_{j=1}^{n_B} \frac{|\mathbf{p}_j^B|^2}{2m_B} + \Psi(\{\mathbf{r}_i^A\}, \{\mathbf{r}_j^B\}), \quad (2)$$

where m_A and m_B are the masses of A and B. The overall interaction potential $\Psi(\{\mathbf{r}_i^A\}, \{\mathbf{r}_j^B\})$ (detailed in the Supplemental Material [31]) governs free movement of A and B and formation of the AB₂ complex.

We define the instantaneous number \hat{n} of AB₂ complexes as:

$$\hat{n}(\Gamma_A, \Gamma_B) = \sum_{i=1}^{n_A} \delta_{q_i, 2}, \quad (3)$$

$$q_i = \sum_{j=1}^{n_B} \Theta(r_0 - |\mathbf{r}_i^A - \mathbf{r}_j^B|) \sum_{i' \neq i} [1 - \Theta(r_0 - |\mathbf{r}_{i'}^A - \mathbf{r}_j^B|)], \quad (4)$$

where r_0 is a distance between A and B used to identify molecular complex AB₂, q_i is the number of B molecules trapped by the i -th A molecule, $\delta_{a,b}$ is the Kronecker delta, and $\Theta(r)$ is the Heaviside step function. In this Letter, we focus on a simplified example using a single

* equally contributed author

† equally contributed author; a.yoshida.phys@gmail.com

‡ takenobu.nakamura@aist.go.jp

§ naoko.nakagawa.phys@vc.ibaraki.ac.jp

parameter r_0 as the discriminant criterion, as given by (4). The complexity in discriminating molecular complexes depends on both the form of the interaction potential $\Psi(\{\mathbf{r}_i^A\}, \{\mathbf{r}_i^B\})$ and the structure of the molecular complex of interest.

In numerical demonstrations, we use the Hamiltonian described in [31] with $4\sigma_{AB} = 2\sigma_B = \sigma_A$, where σ_A and σ_B are the characteristic lengths for repulsive A–A and B–B interactions, respectively [32]. The molecular complex AB_2 is identified using $r_0 = 1.5\sigma_{AB}$.

We next consider a mixture composed of A, B, and C molecules, where C represents a triatomic molecule formed by the irreversible reaction



The structures of both AB_2 and C are shown schematically in the top-left panel of Fig. 1. We assume that the reaction (5) does not occur under ordinary conditions and requires an external energy input, such as instantaneous laser irradiation. C is a stable species, whereas AB_2 is a transient species formed through reversible association.

When C is present, the A molecules in the mixture can be classified into two types: A molecules within C molecules and unbound A molecules (either free A molecules or A molecules within AB_2 complexes). Let n_C denote the number of C molecules. Consequently, there are n_C molecules of A within C and $2n_C$ molecules of B within C. The number of unbound A and B molecules are then $n_A - n_C$ and $n_B - 2n_C$, respectively. To distinguish between these, we re-index the molecules as follows: The microstates of bound and unbound A molecules are denoted by $\Gamma_A^- \equiv (\mathbf{r}_i^A, \mathbf{p}_i^A)_{i=1}^{n_C}$ and $\Gamma_A^\neq \equiv (\mathbf{r}_i^A, \mathbf{p}_i^A)_{i=n_C+1}^{n_A}$, respectively. The two B molecules tightly bound to the i -th A molecule are indexed by $j = 2i - 1$ and $2i$. The microstates of these bound B molecules are denoted by $\Gamma_B^- \equiv (\mathbf{r}_{2i-1}^B, \mathbf{r}_{2i}^B, \mathbf{p}_{2i-1}^B, \mathbf{p}_{2i}^B)_{i=1}^{n_C}$, while the microstates of the unbound B molecules are denoted by $\Gamma_B^\neq \equiv (\mathbf{r}_j^B, \mathbf{p}_j^B)_{j=2n_C+1}^{n_B}$.

We introduce a Hamiltonian H_C to describe the system of n_C molecules of C:

$$H_C(\Gamma_A^-, \Gamma_B^-; n_C) = H_0(\Gamma_A^-, \Gamma_B^-) + \sum_{i=1}^{n_C} \phi_b(\mathbf{r}_{2i-1}^B, \mathbf{r}_{2i}^B; \mathbf{r}_i^A), \quad (6)$$

where ϕ_b represents the binding potential such as

$$\phi_b(\mathbf{r}_{2i-1}^B, \mathbf{r}_{2i}^B; \mathbf{r}_i^A) = \frac{k}{2} \sum_{j=2i-1}^{2i} (|\mathbf{r}_i^A - \mathbf{r}_j^B| - l)^2 \quad (7)$$

with the bond length $l = \sigma_{AB}$ and bond strength k . The total Hamiltonian H of the mixture is then given by:

$$H(\Gamma_A^-, \Gamma_A^\neq, \Gamma_B^-, \Gamma_B^\neq; n_C) = H_C(\Gamma_A^-, \Gamma_B^-; n_C) + H_0(\Gamma_A^\neq, \Gamma_B^\neq) + h_{\text{int}}(\Gamma_A^-, \Gamma_A^\neq, \Gamma_B^-, \Gamma_B^\neq) \quad (8)$$

where h_{int} accounts for interactions between C molecules and unbound A or B molecules. For dilute gases, the interaction term h_{int} can be neglected.

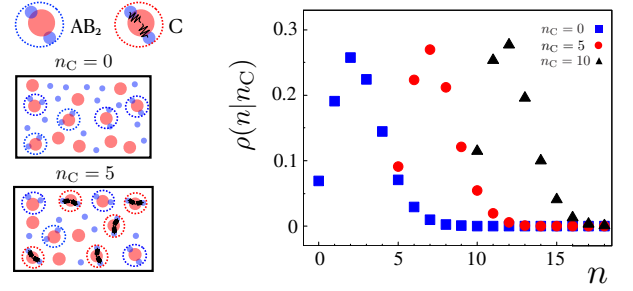


FIG. 1. (Left-top) Structure of individual molecules of AB_2 and C. Dashed circles indicate the discriminant criterion r_0 . (Left-middle and bottom) Schematic snapshots of mixtures: A and B ($n_C = 0$), and A, B, and C ($n_C = 5$). (Right) Density profiles $\rho(n|n_C)$ for $n_C = 0, 5, 10$ at $(n_A, n_B) = (108, 216)$.

Choosing l and k to hold the second derivative of H_0 around $|\mathbf{r}_i^A - \mathbf{r}_{2i}^B| = |\mathbf{r}_i^A - \mathbf{r}_{2i-1}^B| = \sigma_{AB}$, the equilibrium structure of AB_2 remain virtually unchanged. Consequently, AB_2 becomes indistinguishable from C based solely on the discriminant criterion r_0 . For example, in the low-temperature regime, we can design the equation of state such that it remains invariant under the replacement of all AB_2 complexes with C molecules. See [31] for further details.

We extend the definition of the observable \hat{n} from (3) to account for the presence of C:

$$\hat{n}(\Gamma_A^\neq, \Gamma_B^\neq) = n_C + \sum_{i=n_C+1}^{n_A} \delta_{q_i, 2}. \quad (9)$$

The probability density $\rho(n|n_C)$ of observing n molecules of AB_2 and C is formally given by

$$\rho(n|n_C) = \int d\Gamma_A^- d\Gamma_A^\neq d\Gamma_B^- d\Gamma_B^\neq \delta_{n, \hat{n}(\Gamma_A^\neq, \Gamma_B^\neq)} \frac{e^{-\beta H(\Gamma_A^-, \Gamma_A^\neq, \Gamma_B^-, \Gamma_B^\neq; n_C)}}{Z(n_C)}, \quad (10)$$

with the partition function

$$Z(n_C) = \int d\Gamma_A^- d\Gamma_A^\neq d\Gamma_B^- d\Gamma_B^\neq e^{-\beta H(\Gamma_A^-, \Gamma_A^\neq, \Gamma_B^-, \Gamma_B^\neq; n_C)}. \quad (11)$$

Fluctuations in AB_2 abundance: In the following discussion, we fix (T, V, n_A, n_B) , assuming coexistence of the molecular complex AB_2 with free A and B, and the validity of the discriminant criterion r_0 . Refer to [31] for the selection of these parameters. Schematic representations of the mixture are shown on the left-hand side of Fig. 1.

The right panel of Fig. 1 depicts $\rho(n|n_C)$ for three values of n_C , obtained from molecular dynamics simulations. Although the peak of $\rho(n|n_C)$ shifts as n_C increases, the AB_2 density remains nearly constant, since n counts both C and AB_2 molecules as in (9). The density of AB_2 remains relatively constant, irrespective of the amount of C. Instead, this shift indicates a pressure

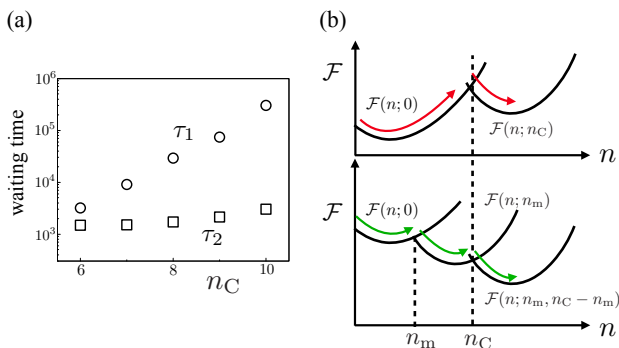


FIG. 2. (a) Waiting times τ_1 and τ_2 with $n_m = 5$ to obtain n_C molecules of C. (b) Typical trajectories on the effective potentials for single-pulse (top) and two-pulse (bottom) operations.

decrease with increasing n_C , demonstrating that systems with $n_C = 0$ and $n_C \neq 0$ are thermodynamically distinct. However, from a mechanical perspective, these systems are nearly equivalent in terms of their instantaneous configurations, exhibiting no significant differences.

Autocatalysis promoting molecular complex: We assume that the irreversible reaction (5) occurs upon instantaneous laser irradiation of AB_2 as an example. Accordingly, we express the type of external operations as single-pulse and two-pulse operations while the idea itself can be extended to other situations. We compare single- and two-pulse operations for producing n_C molecules of C. In the former, n_C complexes must form simultaneously. In the latter, n_m complexes form first, and after relaxation, another $n_C - n_m$ complexes form. Molecular dynamics simulations reveal a significantly higher yield with the two-pulse operation, suggesting autocatalysis. Figure 2(a) compares waiting times to obtain n_C molecules of C.

We elucidate the enhanced reaction rate via $\rho(n|n_C)$. Let τ_1 and τ_2 be mean waiting times for the single- and two-pulse operations, respectively. Defining $\mathcal{F}(n; n_C)$ as an effective potential governing the fluctuations of n , and $n_*(n_C)$ as the most probable value of n ,

$$\rho(n|n_C) \propto e^{-\beta\mathcal{F}(n; n_C)}, \quad (12)$$

$$n_*(n_C) = \arg \min_n \mathcal{F}(n; n_C), \quad (13)$$

the waiting time, $\tau(n_C)$, is defined as the mean first passage time from $n_*(n_C)$ to a given value of n ,

$$\tau(n_C) \propto e^{\beta[\mathcal{F}(n; n_C) - \mathcal{F}(n_*(n_C); n_C)]}. \quad (14)$$

according to Kramers' rate theory [11, 12].

From (14), we obtain

$$\tau_1 \propto \frac{\rho(n_*(0)|0)}{\rho(n_C|0)} \quad (15)$$

for the single-pulse, and

$$\tau_2 \propto \frac{\rho(n_*(0)|0)}{\rho(n_m|0)} + \frac{\rho(n_*(n_m)|n_m)}{\rho(n_C|n_m)} \quad (16)$$

for the two-pulse, where the first term represents the waiting time for n_m complexes to appear simultaneously, and the second term is the waiting time for the subsequent formation of $n_C - n_m$ complexes. Choosing $n_m \sim n_C - n_m$, the two terms in (16) become comparable. With $\rho(n_C|n_m) \sim \rho(n_m|0)$, we approximate $\tau_2 \propto \rho(n_*(0)|0)/\rho(n_C|n_m)$. Thus,

$$\frac{\tau_1}{\tau_2} \propto \frac{\rho(n_C|n_m)}{\rho(n_C|0)} \gg 1, \quad (17)$$

when n_C is not too small.

The estimate (17) indicates significantly faster C production via the two-pulse operation, where initial products catalyze subsequent reactions.

Combinatorial enhancement: We express the promotion rate, τ_1/τ_2 , in terms of \mathcal{F} . We define $n_* \equiv n_*(n_C)$ and $\rho_* \equiv \rho(n_*(n_C)|n_C)$. Equation (12) becomes

$$\rho(n|n_C) = \rho_* e^{-\beta[\mathcal{F}(n; n_C) - \mathcal{F}(n_*; n_C)]}. \quad (18)$$

$\rho(n|n_C)$ is the probability density for a given n_C and is independent of its formation history. For the two-pulse operation, we introduce $\mathcal{F}(n; n_m, n_C - n_m)$ and write

$$\rho(n|n_C) = \rho_* e^{-\beta[\mathcal{F}(n; n_m, n_C - n_m) - \mathcal{F}(n_*; n_m, n_C - n_m)]} \quad (19)$$

analogously to (18). Here, $\mathcal{F}(n; n_C)$ and $\mathcal{F}(n; n_m, n_C - n_m)$ are functions of a single variable n with the parameters after the semicolon held fixed.

Figure 2(b) illustrates the difference between these potentials, with upper and lower panels for single- and two-pulse operations, respectively. The initial $\mathcal{F}(n; 0)$ at $n_C = 0$ is identical for both operations, transitioning to $\mathcal{F}(n; n_C)$ (single-pulse) and $\mathcal{F}(n; n_m)$ (two-pulse). Since binding A and two B requires negligible work, these potentials connect almost continuously to $\mathcal{F}(n; 0)$ at $n = n_C$ and $n = n_m$, respectively. The two-pulse potential undergoes a second transition to $\mathcal{F}(n; n_m, n_C - n_m)$. While the final n_C is the same for both, $\mathcal{F}(n; n_C)$ and $\mathcal{F}(n; n_m, n_C - n_m)$ have the same shape but differ in their vertical offsets. We define this potential difference as

$$F_{\text{gain}}(n_m, n_C) \equiv \mathcal{F}(n; n_C) - \mathcal{F}(n; n_m, n_C - n_m), \quad (20)$$

which is n -independent. F_{gain} characterizes the intermediate state's influence and C's catalytic effect.

We assert that $F_{\text{gain}} \neq 0$ with the following explicit form:

$$F_{\text{gain}}(n_m, n_C) = k_B T \ln \left[\frac{\rho(n_C|n_m)}{\rho(n_C|0)} \frac{\rho(n_m|0)}{\rho(n_m|n_m)} \right] + k_B T \ln \frac{\langle e^{-\beta W(0 \rightarrow n_m)} \rangle_{n_m} \langle e^{-\beta W(n_m \rightarrow n_C)} \rangle_{n_C}}{\langle e^{-\beta W(0 \rightarrow n_C)} \rangle_{n_C}}, \quad (21)$$

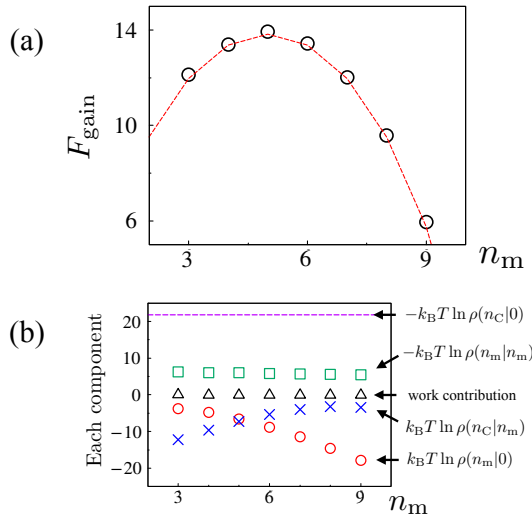


FIG. 3. (a) n_m vs. F_{gain} for $n_C = 10$. The red dashed line is (29). (b) Contributions to F_{gain} from each component in (21).

as derived in End Matter. Here, $\langle \cdot \rangle_{n_C}$ is the ensemble average with $e^{-\beta H} / Z(n_C)$, and

$$W(n \rightarrow n') = \frac{k}{2} \sum_{i=n+1}^{n'} \sum_{j=2i-1}^{2i} (|\mathbf{r}_i^A - \mathbf{r}_j^B| - l)^2 \quad (22)$$

is the work to bind $n' - n$ AB_2 as C. These works are small enough that $\langle W(0 \rightarrow n_m) \rangle_{n_m} + \langle W(n_m \rightarrow n_C) \rangle_{n_C} \simeq \langle W(0 \rightarrow n_C) \rangle_{n_C}$, because (5) occurs only upon AB_2 formation. Thus, Eq. (21) simplifies to

$$F_{\text{gain}} = -k_B T \ln \left[\frac{\rho(n_C|n_m)}{\rho(n_C|0)} \frac{\rho(n_m|0)}{\rho(n_m|n_m)} \right]. \quad (23)$$

Comparing Eqs. (23) and (17), we obtain

$$\frac{\tau_1}{\tau_2} \sim K e^{\beta F_{\text{gain}}} \quad (24)$$

where $K \equiv \rho(n_m|0) / \rho(n_m|n_m)$.

The thermodynamic free energy corresponds to

$$F(n_C) = \mathcal{F}(n_*, n_C), \quad (25)$$

which is given by

$$F(n_C) = -k_B T \ln \frac{Z(n_C)}{(n_A - n_C)! n_C! (n_B - 2n_C)! 2^{n_C}} \quad (26)$$

from standard statistical mechanics, where the factorials account for indistinguishability of unbound A, B, and C molecules, respectively. The 2^{n_C} factor arises from the two B molecules within each C.

$\mathcal{F}(n_*, n_m, n_C - n_m)$ differs from $F(n_C)$ if $F_{\text{gain}} \neq 0$, although n_* is the same for given n_A , n_B , and n_C . This difference arises from the distinguishable reaction history:

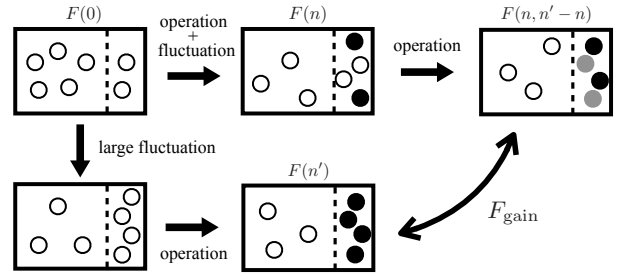


FIG. 4. Schematic of a simpler system exhibiting reduced waiting time, analogous to osmotic pressure. See text.

n_m molecules from the first step and $n_C - n_m$ from the second are distinct. Thus, we define

$$F(n_m, n_C - n_m) = -k_B T \times \ln \frac{Z(n_C)}{(n_A - n_C)! (n_C - n_m)! n_m! (n_B - 2n_C)! 2^{n_C}}, \quad (27)$$

where $Z(n_m, n_C - n_m) = Z(n_C)$ (Ref. [31]). Referring to (25), we suppose

$$F(n_m, n_C - n_m) = \mathcal{F}(n_*, n_m, n_C - n_m). \quad (28)$$

Substituting (25), (26), (27), and (28) into (20) yields

$$F_{\text{gain}} = k_B T \ln \left[\frac{n_C!}{n_m! (n_C - n_m)!} \right]. \quad (29)$$

We examine (29) using molecular dynamics. From trajectories, we determine the four $\rho(n'|n)$ in (21) via (4), (9), and (10), and the three works, $W(0 \rightarrow n_m)$, $W(n_m \rightarrow n_C)$, and $W(0 \rightarrow n_C)$. Figure 3 shows good agreement between numerical results and (29), with the total work contribution (second term in (21)) negligible as expected.

Concluding remarks: We have shown how prior products influence subsequent reaction rates, quantifying this influence via F_{gain} for n_m preceding products. In the thermodynamic limit, F_{gain} reflects the mixing entropy difference between *reactants* and products, arising from the combinatorial enhancement due to molecular indistinguishability. Although indistinguishable in the final mixture, the time to reach a target concentration reveals the reaction's history. This effect may enhance small molecule-protein binding and influence collective antibody behavior, though these are future research directions.

The product increase resembles osmotic pressure across a membrane (Fig. 4), permeable to white molecules but not black. Consider an alchemical operation converting one white molecule to black in the right compartment. The operation triggers diffusion, eventually converting most to black, confined to the right. This initially improbable configuration becomes feasible due to the induced change; F_{gain} quantifies this.

We propose testing this via pulsed laser irradiation. Controlling pulse number and timing mimics the two-pulse protocol. Comparing times to reach a target C concentration with single- and multi-pulse irradiation for different n_m should reveal the predicted waiting time reduction, directly demonstrating the combinatorial enhancement of autocatalysis. The laser frequency should match reaction (5); pulse duration should be shorter than the

molecular association timescale.

Acknowledgement The authors thank T. Kanazawa, N. Matubayashi, and Y. Nakayama for useful discussions and S.-i. Sasa for critical reading of the manuscript. The numerical simulations were performed with LAMMPS on the supercomputer at ISSP at the University of Tokyo. This study was supported by JSPS KAKENHI Grant Numbers JP23K22415.

-
- [1] Max F. Perutz, Mechanisms of cooperativity and allosteric regulation in proteins, *Q. Rev. Biophys.* 22, 2 (1989). DOI: 10.1017/s0033583500003826
- [2] Charles A. Janeway Jr., Paul Travers, Mark Walport, and Mark J. Shlomchik. *Immunobiology: The immune system in health and disease*, 5th ed. (Garland Science, New York, 2001).
- [3] Jacques Monod, Jeffries Wyman, and Jean-Pierre Changeux. On the nature of allosteric transitions: a plausible model. *J. Mol. Biol.* 12(1), 88-118 (1965). DOI: 10.1016/s0022-2836(65)80285-6
- [4] Daniel E. Koshland Jr., George Némethy, and David L. Filmer, Comparison of experimental binding data and theoretical models in proteins containing subunits, *Biochem.* 5, 365-385 (1966). DOI: 10.1021/bi00865a047
- [5] Daniel E. Koshland Jr. and Kambiz Hamadani, Proteomics and Models for Enzyme Cooperativity, *J. Biol. Chem.* 277, 46841-46844 (2002). DOI: 10.1074/jbc.R200014200
- [6] Qiang Cui and Martin Karplus, Allostery and cooperativity revisited, *Protein Sci.* 17, 1295-1307 (2008). DOI: 10.1110/ps.03259908
- [7] Albert Goldbeter, *Biochemical oscillations and cellular rhythms: the molecular bases of periodic and chaotic behaviour.* (Cambridge Univ. Press, Cambridge, 1996).
- [8] John Tyson, Katherine C. Chen, and Bela Novak, Sniffers, buzzers, toggles and blinkers: dynamics of regulatory and signaling pathways in the cell. *Curr. Opin. Cell Biol.* 15, 221-231 (2003). DOI: 10.1016/S0955-0674(03)00017-6
- [9] Svante Arrhenius, Über die Dissociationswärme und den Einfluß der Temperatur auf den Dissociationsgrad der Elektrolyte, *Z. Phys. Chem.* 4, 96-116 (1889). DOI: 10.1515/zpch-1889-0408
- [10] Henry Eyring, The Activated Complex in Chemical Reactions, *J. Chem. Phys.* 3, 107 (1935). DOI: 10.1063/1.1749604
- [11] Hendrik A. Kramers, Brownian motion in a field of force and the diffusion model of chemical reactions, *Physica* 7, 284 (1940). DOI: 10.1016/S0031-8914(40)90098-2
- [12] Peter Hänggi, Peter Talkner, and Michal Borkovec, Reaction-rate theory: fifty years after Kramers, *Rev. Mod. Phys.* 62, 251 (1990). DOI: 10.1103/RevModPhys.62.251
- [13] Denis J. Evans, Ezechiel G. Cohen, and Gary P. Morriss, Probability of Second Law Violations in Shearing Steady States, *Phys. Rev. Lett.* 71, 3616 (1993). DOI: 10.1103/PhysRevLett.71.2401
- [14] Giovanni Gallavotti and Ezechiel godert Cohen, Dynamical ensembles in stationary states, *J. Stat. Phys.* 80, 931-970 (1995). DOI: 10.1007/BF02179860
- [15] Jorge Kurchan, Fluctuation theorem for stochastic dynamics, *J. Phys. A Math. Gen.* 31, 3719 (1998). DOI: 10.1088/0305-4470/31/16/003
- [16] Christopher Jarzynski, Hamiltonian Derivation of a Detailed Fluctuation Theorem, *J. Stat. Phys.* 98, 77-102 (2000). DOI: 10.1023/A:1018670721277
- [17] Christian Maes, The Fluctuation Theorem as a Gibbs Property, *J. Stat. Phys.* 95, 367-392 (1999). DOI: 10.1023/A:1004541830999
- [18] Ken Sekimoto, *Stochastic Energetics*, (Lect. Notes Phys., Springer, 2010).
- [19] Udo Seifert, Stochastic thermodynamics, fluctuation theorems and molecular machines, *Rep. Prog. Phys.* 75, 126001 (2012). DOI: 10.1088/0034-4885/75/12/126001
- [20] Takahiro Sagawa and Masahito Ueda, Second Law of Thermodynamics with Discrete Quantum Feedback Control, *Phys. Rev. Lett.* 100, 080403 (2008). DOI: 10.1103/PhysRevLett.100.080403
- [21] Takahiro Sagawa and Masahito Ueda, Minimal Energy Cost for Thermodynamic Information Processing: Measurement and Information Erasure, *Phys. Rev. Lett.* 102, 250602 (2009). DOI: 10.1103/PhysRevLett.102.250602
- [22] Jordan M. Horowitz, Takahiro Sagawa, and Juan M. R. Parrondo, Imitating Chemical Motors with Optimal Information Motors, *Phys. Rev. Lett.* 111, 010602 (2013). DOI: 10.1103/PhysRevLett.111.010602
- [23] Kyogo Kawaguchi, Shin-ichi Sasa, and Takahiro Sagawa, Nonequilibrium dissipation-free transport in F₁-ATPase and the thermodynamic role of asymmetric allostery, *Biophys J.* 106, 2450-2457 (2014). DOI: 10.1016/j.bpj.2014.04.034
- [24] Yûto Murashita, Ken Funo, and Masahito Ueda, Nonequilibrium equalities in absolutely irreversible processes. *Phys. Rev. E* 90, 042110 (2014). DOI: 10.1103/PhysRevE.90.042110
- [25] Yûto Murashita and Masahito Ueda, Gibbs paradox revisited from the fluctuation theorem with absolute irreversibility. *Phys. Rev. Lett.* 118, 060601 (2017). DOI: 10.1103/PhysRevLett.118.060601
- [26] Akira Yoshida and Naoko Nakagawa, Work relation for determining the mixing free energy of small-scale mixtures, *Phys. Rev. Res.* 4, 023119 (2022). DOI: 10.1103/PhysRevResearch.4.023119
- [27] Shin-ichi Sasa, Ken Hiura, Naoko Nakagawa, Akira Yoshida, Quasi-static Decomposition and the Gibbs Factorial in Small Thermodynamic Systems, *Journal of Stat. Phys.* 189, 31 (2022). DOI: 10.1007/s10955-022-02991-7
- [28] Ken Sekimoto, Autonomous free-energy transducer working under thermal fluctuations, *Physica D*, 205, 242-248 (2005). DOI: 10.1016/j.physd.2005.01.013

- [29] Takahiro Harada and Naoko Nakagawa, A reversibility parameter for a Markovian stepper, EPL, 78, 50002 (2007). DOI: 10.1209/0295-5075/78/50002
- [30] Pieter Baerts, Urna Basu, Christian Maes, and Soghra Safaverdi, Frenetic origin of negative differential response, Phys. Rev. E 88, 052109 (2013). DOI: 10.1103/PhysRevE.88.052109
- [31] See Supplemental Material at [URL will be inserted by publisher] for detailed explanations, supplemental parameters, numerical data, and derivations, which includes

- Refs. [32–34].
- [32] Takenobu Nakamura, in preparation.
- [33] John D. Weeks, David Chandler, and Hans C. Andersen, Role of Repulsive Forces in Determining the Equilibrium Structure of Simple Liquids, J. Chem. Phys. 54, 5237 (1971). DOI: 10.1063/1.1674820
- [34] Frank H. Stillinger and Thomas A. Weber, Computer simulation of local order in condensed phases of silicon, Phys. Rev. B. 31, 5262 (1985). DOI: 10.1103/PhysRevB.31.5262

End Matter

Appendix : Derivation of Eq. (21)

We set the initial amount of C to be n and then perform a feedback protocol to bind $n' - n$ molecules from AB_2 to C when the amount of AB_2 is equal to $n' - n$. The resulting amount of C is n' . Below, we consider C to be distinguishable between the newly formed $n' - n$ molecules and the initial n molecules. We denote the microstate after the feedback protocol as $\Gamma^{(n, n'-n)} = (\Gamma_A^{==}, \Gamma_A^{\neq=}, \Gamma_A^{\neq\neq}, \Gamma_B^{==}, \Gamma_B^{\neq=}, \Gamma_B^{\neq\neq})$ where

$$\begin{aligned}\Gamma_A^{==} &= (\mathbf{r}_i^A, \mathbf{p}_i^A)_{i=1}^n, & \Gamma_B^{==} &= (\mathbf{r}_{2i-1}^B, \mathbf{r}_{2i}^B, \mathbf{p}_{2i-1}^B, \mathbf{p}_{2i}^B)_{i=1}^n, \\ \Gamma_A^{\neq=} &= (\mathbf{r}_i^A, \mathbf{p}_i^A)_{i=n+1}^{n'}, & \Gamma_B^{\neq=} &= (\mathbf{r}_{2i-1}^B, \mathbf{r}_{2i}^B, \mathbf{p}_{2i-1}^B, \mathbf{p}_{2i}^B)_{i=n+1}^{n'}, \\ \Gamma_A^{\neq\neq} &= (\mathbf{r}_i^A, \mathbf{p}_i^A)_{i=n'+1}^{n_A}, & \Gamma_B^{\neq\neq} &= (\mathbf{r}_j^B, \mathbf{p}_j^B)_{j=2n'+1}^{n_B}.\end{aligned}$$

That is, $\Gamma_A^{\neq=}$ and $\Gamma_B^{\neq=}$ specify the microstates for the newly formed $n' - n$ molecules of C. $\Gamma_A^{==}$ and $\Gamma_B^{==}$ are the microstates for the initial n molecules of C, and $\Gamma_A^{\neq\neq}$ and $\Gamma_B^{\neq\neq}$ are the microstates for the unbound A and B molecules throughout the protocol.

Suppose the time evolution is Markovian with the transition probability $\mathcal{T}_{(n)}(\hat{\Gamma})$ for a path $\hat{\Gamma}$ with n molecules of C. Let t_m be the time at which $n' - n$ molecules of AB_2 bind to form C. Precisely, the A and B molecules to be bound as C at $t = t_m$ are not yet identified for $t < t_m$. By picking out the trajectories that have $n' - n$ complexes AB_2 at $t = t_m$, we denote the microstate at $t > t_m$ as $\Gamma^{(n, n'-n)}(t)$ and define a path $\hat{\Gamma}_>$ for $t_m < t \leq t_{\text{fin}}$ as $\hat{\Gamma}_> \equiv (\Gamma^{(n, n'-n)}(t))_{t \in (t_m, t_{\text{fin}}]}$. We extend it to $t_{\text{ini}} \leq t < t_m$ as $\hat{\Gamma}_< = (\Gamma^{(n, n'-n)}(t))_{t \in [t_{\text{ini}}, t_m)}$. The entire path is then written as $\hat{\Gamma}_{n \rightarrow n'} = (\hat{\Gamma}_<, \hat{\Gamma}_>)$, and its time-reversed path as $\hat{\Gamma}_{n' \rightarrow n}^\dagger = (\hat{\Gamma}_>^\dagger, \hat{\Gamma}_<^\dagger)$. The local detailed balance condition is then

$$\frac{\mathcal{T}_{(n)}(\hat{\Gamma}_<) \mathcal{T}_{(n')}(\hat{\Gamma}_>)}{\mathcal{T}_{(n')}(\hat{\Gamma}_>^\dagger) \mathcal{T}_{(n)}(\hat{\Gamma}_<^\dagger)} = e^{-\beta Q}, \quad (\text{A1})$$

where

$$Q = H(\Gamma^{(n, n'-n)}(t_{\text{fin}}); n') - H(\Gamma^{(n, n'-n)}(t_{\text{ini}}); n) - W(\Gamma^{(n, n'-n)}(t_m)), \quad (\text{A2})$$

and $W(\Gamma^{(n, n'-n)}(t_m)) = W(n \rightarrow n')$ given in Eq. (22) for $n' - n$ molecules to be bound instantaneously at $t = t_m$. Multiplying both sides of (A1) by Kronecker's delta leads to

$$\begin{aligned}e^{-\beta H(\Gamma^{(n, n'-n)}(t_{\text{ini}}); n)} \mathcal{T}_{(n)}(\hat{\Gamma}_<) \delta_{n', \hat{n}(\Gamma^{(n, n'-n)}(t_m))} e^{-\beta W(\Gamma^{(n, n'-n)}(t_m))} \mathcal{T}_{(n')}(\hat{\Gamma}_>) \\ = e^{-\beta H(\Gamma^{(n, n'-n)}(t_{\text{fin}}); n')} \mathcal{T}_{(n')}(\hat{\Gamma}_>^\dagger) \delta_{n', \hat{n}(\Gamma^{(n, n'-n)}(t_m))} \mathcal{T}_{(n)}(\hat{\Gamma}_<^\dagger),\end{aligned} \quad (\text{A3})$$

Integrating (A3) over all paths, $\int \mathcal{D}\hat{\Gamma}_< \mathcal{D}\hat{\Gamma}_>$, yields

$$\int d\Gamma^{(n, n'-n)} \delta_{n', \hat{n}(\Gamma^{(n, n'-n)})} e^{-\beta W(\Gamma^{(n, n'-n)})} e^{-\beta H(\Gamma^{(n, n'-n)}; n)} = Z(n') \rho(n' | n') \quad (\text{A4})$$

by performing the path integral and using Eqs. (10) and (11). See Ref. [31] for the step-by-step transformations.

The natural expression of the microstates with n molecules of C is $\Gamma^{(n, 0)} = (\Gamma_A^{\neq=}, \Gamma_A^{\neq\neq}, \Gamma_B^{\neq=}, \Gamma_B^{\neq\neq})$ rather than $\Gamma^{(n, n'-n)}$. They are connected by $\Gamma_A^{\neq} = (\Gamma_A^{\neq=}, \Gamma_A^{\neq\neq})$, $\Gamma_B^{\neq} = (\Gamma_B^{\neq=}, \Gamma_B^{\neq\neq})$, $\Gamma_A^{\neq=} = \Gamma_A^{\neq}$, and $\Gamma_B^{\neq=} = \Gamma_B^{\neq}$, and therefore, changing the

notations from $\Gamma^{(n,n'-n)}$ to $\Gamma^{(n,0)}$ in (A4), we need to consider the difference in distinguishability in Γ_A^\neq and Γ_B^\neq . Using $H(\Gamma^{(n,n'-n)}; n) = H(\Gamma^{(n,0)}; n)$, and $W(\Gamma^{(n,n'-n)}) = W(\Gamma^{(n,0)})$ under the constraint $\hat{n}(\Gamma^{(n,n'-n)}) = \hat{n}(\Gamma^{(n,0)}) = n$, the left-hand side of (A4) is rewritten as

$$\left[\frac{(n_A - n)!}{(n_A - n')!(n' - n)!} \frac{(n_B - 2n)!}{(n_B - 2n')! 2^{n'-n}} \right]^{-1} \int d\Gamma^{(n,0)} \delta_{n', \hat{n}(\Gamma^{(n,0)})} e^{-\beta W(\Gamma^{(n,0)})} e^{-\beta H(\Gamma^{(n,0)}; n)}. \quad (\text{A5})$$

Here, the integral in (A5) is calculated as $Z(n)\rho(n'|n)\langle e^{-\beta W(n \rightarrow n')} \rangle_{n'}$ by using Eqs. (10) and (11). Thus, (A4) results in

$$e^{-\beta F(n)} \rho(n'|n) \langle e^{-\beta W(n \rightarrow n')} \rangle_{n'} = e^{-\beta F(n, n'-n)} \rho(n'|n'), \quad (\text{A6})$$

where $F(n)$ and $F(n, n'-n)$ are defined in Eqs. (26) and (27), respectively.

For three cases $(n, n') = (0, n_m)$, (n_m, n_C) , and $(0, n_C)$, Eq. (A6) yields

$$\begin{aligned} e^{-\beta F(0)} \rho(n_m|0) \langle e^{-\beta W(0 \rightarrow n_m)} \rangle_{n_m} &= e^{-\beta F(0, n_m)} \rho(n_m|n_m), \\ e^{-\beta F(n_m)} \rho(n_C|n_m) \langle e^{-\beta W(n_m \rightarrow n_C)} \rangle_{n_C} &= e^{-\beta F(n_m, n_C - n_m)} \rho(n_C|n_C), \\ e^{-\beta F(0)} \rho(n_C|0) \langle e^{-\beta W(0 \rightarrow n_C)} \rangle_{n_C} &= e^{-\beta F(0, n_C)} \rho(n_C|n_C), \end{aligned}$$

respectively. Note that $F(0, n) = F(n)$. Multiplying the first and second relations and dividing by the third relation, we obtain the formula for F_{gain} as Eq. (21) with $F_{\text{gain}}(n_m, n_C) \equiv F(n_C) - F(n_m, n_C - n_m)$, which corresponds to the definition in Eq. (20) when $n = n_*(n_C)$.

Supplemental Material for “Autocatalysis due to combinatorial enhancement”

Nanako Hirano¹, Akira Yoshida^{1,2}, Takenobu Nakamura³, and Naoko Nakagawa¹

¹*Department of Physics, Ibaraki University, Mito 310-8512, Japan*

²*Department of Physics, Kyoto University, Kyoto, 606-8502 Japan*

³*National Institute of Advanced Industrial Science and Technology (AIST), Tsukuba 305-8568, Japan*

The Supplemental Material consists of seven appendices. Supplement I describes the Hamiltonian adopted for the numerical demonstrations in the main text. The setup for molecular dynamics simulations and the thermodynamic properties obtained are illustrated in Supplement II. The choices of the criterion r_0 and the temperature T are examined in Supplement III and Supplement IV, respectively. Supplement V and Supplement VI provide the explanation of Eq. (27) and additional details for the derivation of Eq. (21) presented in End Matter, respectively. Supplemental figures for Fig. 3 are presented in Supplement VII.

Supplement I: A model Hamiltonian for numerical experiment

For numerical demonstrations, we use a Hamiltonian defined for three-dimensional systems:

$$\begin{aligned}
 H_0(\Gamma_A, \Gamma_B) = & \sum_{i=1}^{n_A} \frac{|\mathbf{p}_i^A|^2}{2m_A} + \sum_{j=1}^{n_B} \frac{|\mathbf{p}_j^B|^2}{2m_B} + \sum_{i_1=1}^{n_A} \sum_{i_2>i_1}^{n_A} \phi^{\text{WCA}}(|\mathbf{r}_{i_1}^A - \mathbf{r}_{i_2}^A|; \sigma_A) + \sum_{j_1=1}^{n_B} \sum_{j_2>j_1}^{n_B} \phi^{\text{WCA}}(|\mathbf{r}_{j_1}^B - \mathbf{r}_{j_2}^B|; \sigma_B) \\
 & + \sum_{i=1}^{n_A} \sum_{j=1}^{n_B} \phi_2^{\text{SW}}(|\mathbf{r}_i^A - \mathbf{r}_j^B|; \sigma_{AB}) + \sum_{i=1}^{n_A} \sum_{j_1=1}^{n_B} \sum_{j_2>j_1}^{n_B} \phi_3^{\text{SW}}(|\mathbf{r}_i^A - \mathbf{r}_{j_1}^B|, |\mathbf{r}_i^A - \mathbf{r}_{j_2}^B|, \theta_{j_1 i j_2}; \sigma_{AB}, \theta_0) \quad (\text{I.1})
 \end{aligned}$$

with $m_A = m_B = m$, where $\phi^{\text{WCA}}(r; \sigma)$ is the Weeks-Chandler-Andersen (WCA) potential [1]

$$\phi^{\text{WCA}}(r; \sigma) = 4\varepsilon \left[\left(\frac{\sigma}{r} \right)^{12} - \left(\frac{\sigma}{r} \right)^6 \right] \Theta(2^{1/6}\sigma - r) \quad (\text{I.2})$$

describing the two-body softcore-repulsive interaction with diameter σ and step function $\Theta(r)$. $\phi_2^{\text{SW}}(r; \sigma)$ and $\phi_3^{\text{SW}}(r, r', \theta; \sigma, \theta_0)$ are the two-body and three-body interaction potentials of the Stillinger-Weber (SW) potential [2],

$$\phi_2^{\text{SW}}(r; \sigma) = A\varepsilon \left[B \left(\frac{\sigma}{r} \right)^p - \left(\frac{\sigma}{r} \right)^q \right] \exp\left(\frac{\sigma}{r - 1.5\sigma} \right) \Theta(1.5\sigma - r), \quad (\text{I.3})$$

$$\phi_3^{\text{SW}}(r, r', \theta; \sigma) = \lambda\varepsilon [\cos\theta - \cos\theta_0]^2 \exp\left(\frac{\sigma}{r - 1.5\sigma} \right) \exp\left(\frac{\sigma}{r' - 1.5\sigma} \right) \Theta(1.5\sigma - r)\Theta(1.5\sigma - r'), \quad (\text{I.4})$$

where θ is the angle defined by the three bodies. The dimensionless parameters are set as $A = 200$, $B = 0.50$, $p = 4.0$, $q = 0.0$, and $\lambda = 100$. In the last term of (I.1), $\theta_{j_1 i j_2}$ is the angle formed by the two vectors, $\mathbf{r}_i^A - \mathbf{r}_{j_1}^B$ and $\mathbf{r}_i^A - \mathbf{r}_{j_2}^B$ at the point \mathbf{r}_i^A . $\phi_2^{\text{SW}}(r)$ is repulsive for $r \leq \sigma_{AB}$ and attractive for $\sigma_{AB} < r \leq 1.5\sigma_{AB}$. $\phi_3^{\text{SW}}(r, r', \theta)$ stabilizes the angle $\theta_{j_1 i j_2}$ at θ_0 and acts only when two B molecules are near the i -th A molecule. We choose $\sigma_A = 4.0\sigma$, $\sigma_B = 2.0\sigma$, $\sigma_{AB} = 1.0\sigma$, and $\theta_0 = \pi$ so that the configuration of the molecular association AB_2 matches schematically Fig. S.1(c). See Ref. [3] for details. The interaction potentials between two A, between two B, and between A and B are plotted in Fig. S.1(a) for $\theta = \theta_0$.

As shown in Fig. S.1, the attractive interaction arises solely from $\phi_2^{\text{SW}}(r)$. It provides a minimum at $r \simeq \sigma$, which is the expected distance $|\mathbf{r}_i^A - \mathbf{r}_j^B| \simeq \sigma$ between A and B in AB_2 . Reflecting this minimum, we set the bond length as $l = \sigma$ in (7), i.e.,

$$\phi_b(\mathbf{r}_{2i-1}^B, \mathbf{r}_{2i}^B; \mathbf{r}_i^A) = \frac{k}{2} \sum_{j=2i-1}^{2i} (|\mathbf{r}_i^A - \mathbf{r}_j^B| - \sigma)^2. \quad (\text{I.5})$$

The value of k is chosen as $k = 40\varepsilon/\sigma^2$ such that ϕ_b minimally affects the properties around the minimum of $\phi_2^{\text{SW}}(r)$. See Fig. S.1(b).

Hereafter, we take units $\sigma = 1$, $\varepsilon = 1$, $m = 1$, and $k_B = 1$.

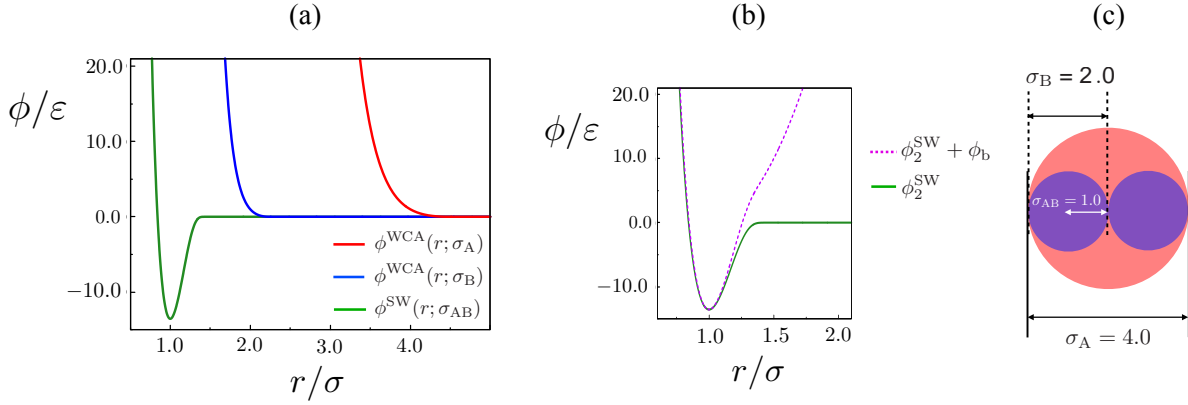


FIG. S.1. (a) Interaction potentials $\phi^{\text{WCA}}(r; \sigma_A)$ (red), $\phi^{\text{WCA}}(r; \sigma_B)$ (blue), and $\phi_2^{\text{SW}}(r; \sigma_{AB})$ (green), with $\sigma_A = 4.0\sigma$, $\sigma_B = 2.0\sigma$, $\sigma_{AB} = 1.0\sigma$, and $\theta_0 = \pi$. $\phi_3^{\text{SW}}(r) = 0$ when $\theta = \theta_0$ or $r > 1.5\sigma$, and $\phi_3^{\text{SW}}(r) > 0$ otherwise. (b) Comparison of $\phi_2^{\text{SW}}(r; \sigma_{AB})$ (green) with $\phi_2^{\text{SW}}(r; \sigma_{AB}) + \phi_b(r)$ (purple dashed). $\phi_b(r)$ does not significantly modify the attractive interaction between A and B near $r/\sigma \simeq 1.0$ but becomes steep with increasing r , ensuring that A and B are bound eternally. In contrast, $\phi_2^{\text{SW}}(r; \sigma_{AB})$ becomes flat for $r/\sigma_{AB} > 1.5$, preventing the maintenance of A-B binding under large fluctuations. (c) Schematic diagram of the molecular association AB_2 with $\sigma = 1.0$.

Supplement II: Molecular dynamics simulations

We perform molecular dynamics simulations in NVT ensembles with the Nosé-Hoover thermostat at temperature T , in a periodic boundary box of volume $V = L_x L_y L_z$ with $L_x : L_y : L_z = 1 : 1 : 1$ and $L_x = 45$, and with $n_A : n_B = 1 : 2$ and $n_A = 108$.

We start with an initial configuration where all A and B molecules form AB_2 complexes, and the AB_2 complexes are arranged in a regular lattice within the box. The initial velocities of all molecules are sampled from the Maxwell distribution at temperature T . A typical relaxation process is shown in Fig. S.2, where \hat{n} is the number of AB_2 molecules, identified using a critical distance $r_0 = 1.5$, at $T = 2.5$. The choice of r_0 is examined later. Figure S.2 exhibits an exponential decay with a relaxation time between 10^2 and 10^3 . We repeated the same procedure for various values of T and determined the sampling time to be from $t = 1.0 \times 10^7$ to 2.0×10^7 with a time interval of 50, i.e., the number of samples for each point is 2.0×10^5 . Hereafter, we denote the sample average as $\langle \cdot \rangle$.

We examine the virial pressure P as the system's pressure. Figure S.3(a) shows the numerical results of P for various values of T . At higher temperatures, P obeys an equation of state,

$$P = \frac{(n_A + n_B)k_B T}{V - (n_A v_A + n_B v_B)}, \quad (\text{II.1})$$

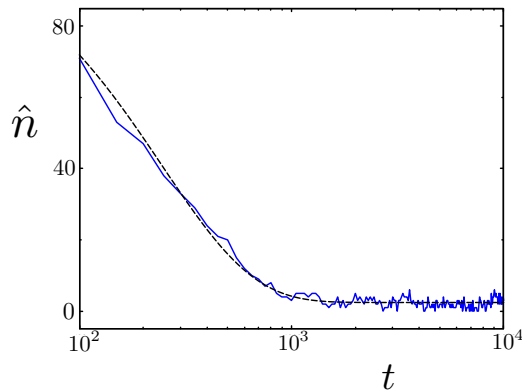


FIG. S.2. Time evolution of \hat{n} with $n_A = 108$, $n_B = 216$, $n_C = 0$, $L_x = L_y = L_z = 45$, and $T = 2.5$. The dashed black line is a fitting curve given by $\hat{n}(t) = a + b \exp(-t/\tau_r)$ with the relaxation time $\tau_r = 245$.

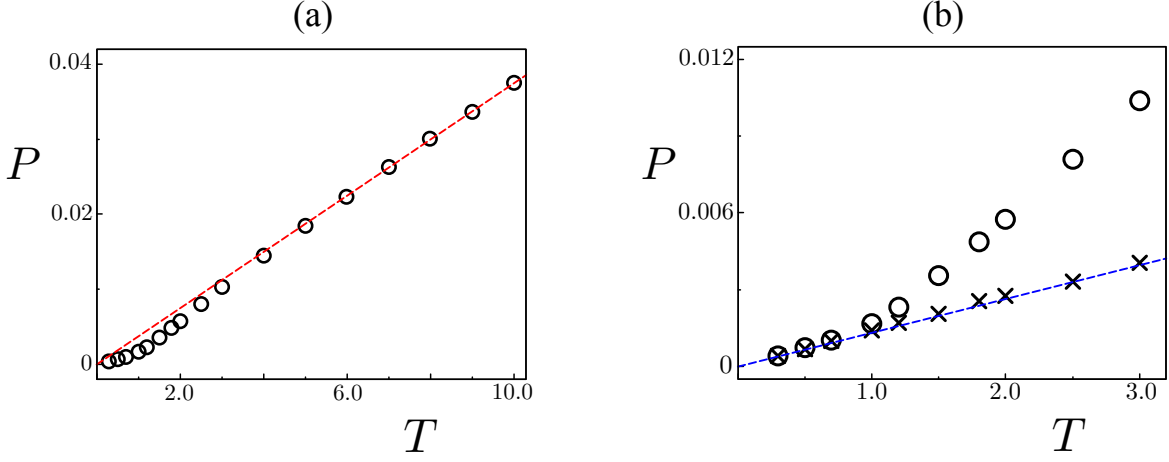


FIG. S.3. (a) Temperature dependence of virial pressure P for $n_C = 0$ (circles). The dashed red line is the equation of state (II.1). (b) Close-up of (a) for $T \leq 3.0$, plotted simultaneously with P obtained in the system with $n_C = n_A$ (crosses). The blue dashed line is an equation of state (II.2).

depicted by the dashed red line, where $v_A = 4\pi(\sigma_A/2)^3/3$ and $v_B = 4\pi(\sigma_B/2)^3/3$. Equation (II.1) is the equation of state for an ideal gas, excluding the volume occupied by the molecules, $n_A v_A + n_B v_B$. The agreement indicates that all A and B molecules are free, and no molecules associate with each other for $T > 4.0$.

Numerical results deviate from (II.1) for $T < 4.0$, implying the existence of molecular complex AB_2 . Figure S.3(b) shows a close-up for the lower temperature region. The blue dashed line corresponds to

$$P = \frac{n_A k_B T}{V - n_A v_C}, \quad (\text{II.2})$$

where n_A is the number of AB_2 complexes when all molecules are associated. v_C is the excluded volume due to one AB_2 complex, determined by the following procedure. We perform molecular dynamics simulations for n_C molecules of C using $n_C = n_A$. Since the molecular structure of C is expected to be almost the same as that of AB_2 but never dissociates, the equation of state for this system should match the lower-temperature behavior of the original system. The crosses in Fig. S.3(b) are the numerical results for the system consisting of C and agree with the circles for the original system at $T < 1.0$. Using the crosses, we determine v_C in (II.2) and obtain $v_C = 85.9$, corresponding to $\sigma_C = 5.47$.

We remark that the agreement of the equations of state between the original system and the system of C confirms the validity of the chosen values of k and l , because these values do not affect the macroscopic properties of the system. Furthermore, both equations of state, (II.1) and (II.2), indicate the system is dilute enough to regard A, B, AB_2 , and C as free particles, except for collisions that occur when any two molecules approach closer than their interaction length.

Supplement III: Criterion r_0 for identifying molecular complex AB_2

Below, we explain why the numerical demonstrations in the main text set the criterion r_0 to 1.5, with which the instantaneous number $\hat{n}(\Gamma_A, \Gamma_B)$ of AB_2 complexes is determined. First, r_0 should be greater than σ_{AB} and less than $(\sigma_A + \sigma_B)/2$, i.e., $1.0 < r_0 < 3.0$, as illustrated in Fig. S.1. The number of AB_2 complexes would always be approximately 0 if we set the criterion as $r_0 < \sigma_{AB}$, which is far from reality.

The average $n \equiv \langle \hat{n} \rangle$ is a function of r_0 and T . Figures S.4 show n as a function of r_0 for $T = 0.5$ and $T = 2.5$. $T = 0.5$ is low enough for all molecules to associate as AB_2 , and the system obeys the equation of state in (II.2). The expected value, $n \simeq n_A$, is obtained when we set $r_0 \geq 1.2$, as shown in Fig. S.4(a). At $T = 2.5$, some A and B molecules associate as forming AB_2 . Correspondingly, Fig. S.4(b) exhibits a stepwise change around $r_0 = 1.2$, consistent with Fig. S.4(a). The value of n is almost unchanged up to $r_0 = 1.7$ and then starts to increase. This increase in n with increasing r_0 is due to misidentification: free B molecules, not influenced by ϕ^{SW} , are occasionally counted as part of AB_2 complexes when two such molecules are near a given A. We thus adopt $r_0 = 1.5$ to distinguish AB_2 .

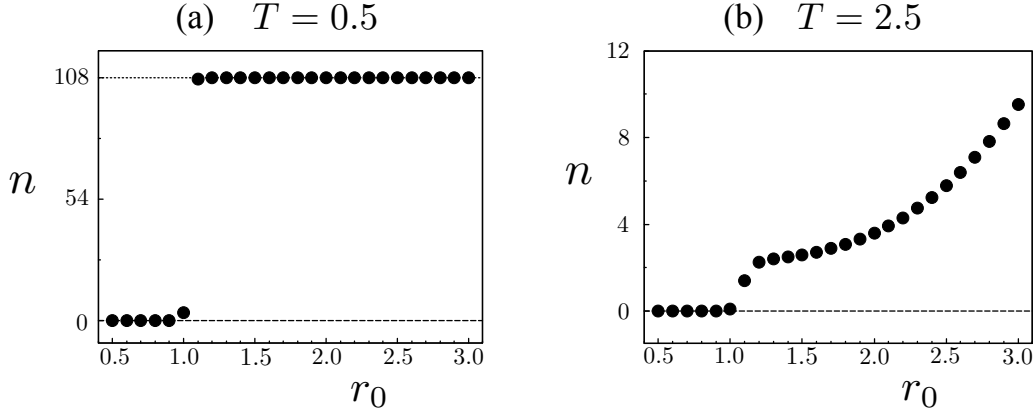


FIG. S.4. Mean number n of A molecules identified as part of AB_2 complexes, for different values of the criterion r_0 when $n_C = 0$. (a) $T = 0.5$ and (b) $T = 2.5$.

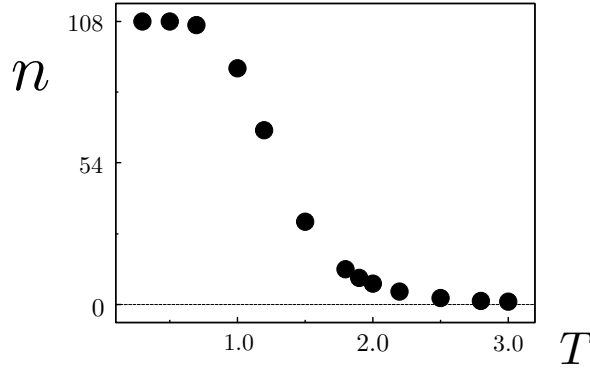


FIG. S.5. n vs. T for $n_C = 0$ with the criterion $r_0 = 1.5$ to distinguish AB_2 from other forms of A. $n \simeq n_A$ for $T < 1.0$, while $n \simeq 0$ for $T \geq 3.0$. Molecular complex AB_2 exists in the range $1.0 \leq T < 3.0$.

Adopting $r_0 = 1.5$, we summarize the dependence of the number, n , of AB_2 complexes on T in Fig. S.5. It shows that the molecules begin to dissociate around $T = 1.0$. We find that the temperature range $1.0 < T < 3.0$ is suitable for observing the coexistence of AB_2 with free A and free B, that is, to observe the reversible reaction $A + 2B \rightleftharpoons AB_2$.

Supplement IV: Choice of T and maximum value of n_C for numerical evaluation of F_{gain}

In the main text, we chose the temperature for the numerical evaluations as $T = 2.5$ at which AB_2 is seldom formed, as shown in Fig. S.5. Below, we demonstrate the advantages of $T = 2.5$ for numerical examinations. We also explain why we set the final amount, n_C , of the product C as $n_C \leq 10$ in our numerical experiments. We emphasize that the requirements illustrated below are purely for numerical convenience, and the theoretical results, Eqs. (21) and (29) in the main text, are independent of these requirements.

To determine F_{gain} , as derived in Eq. (21) in the main text, we need to calculate four probability density values: $\rho(n_C|n_m)$, $\rho(n_C|0)$, $\rho(n_m|0)$, and $\rho(n_m|n_m)$. It is important to choose parameters such that these four quantities are numerically accessible with sufficient statistical accuracy. Let $n_*(0)$ and $n_*(n_m)$ be the most probable values for $\rho(n|0)$ and $\rho(n|n_m)$, respectively. Since we are considering $n_C > n_m > n_*(0)$, and since $n_C - n_*(n_m) < n_C - n_*(0)$ implies $\rho(n_C|0) < \rho(n_C|n_m)$, estimating $\rho(n_C|0)$ with sufficient accuracy requires significantly more samples than estimating $\rho(n_C|n_m)$ or $\rho(n_m|0)$. Thus, the accuracy of $\rho(n_C|0)$ and $\rho(n_m|n_m)$ is crucial for the reliable numerical evaluation of F_{gain} . Figures S.6 plot $\rho(n|n_m)$ for three values of n_m at $T = 2.5$, 2.0, and 1.5, respectively. The magnitude of $\rho(n_m|n_m)$ can be checked by comparing the values at $n - n_m = 0$ (dashed line) in each figure for the three different values of n_m . We find that at $T = 2.5$, $\rho(n_m|n_m)$ can be evaluated with reasonable accuracy. However, at $T = 1.5$, $\rho(n_m|n_m)$ becomes vanishingly small, making accurate evaluation difficult. At $T = 2.0$, evaluating $\rho(n_m|n_m)$

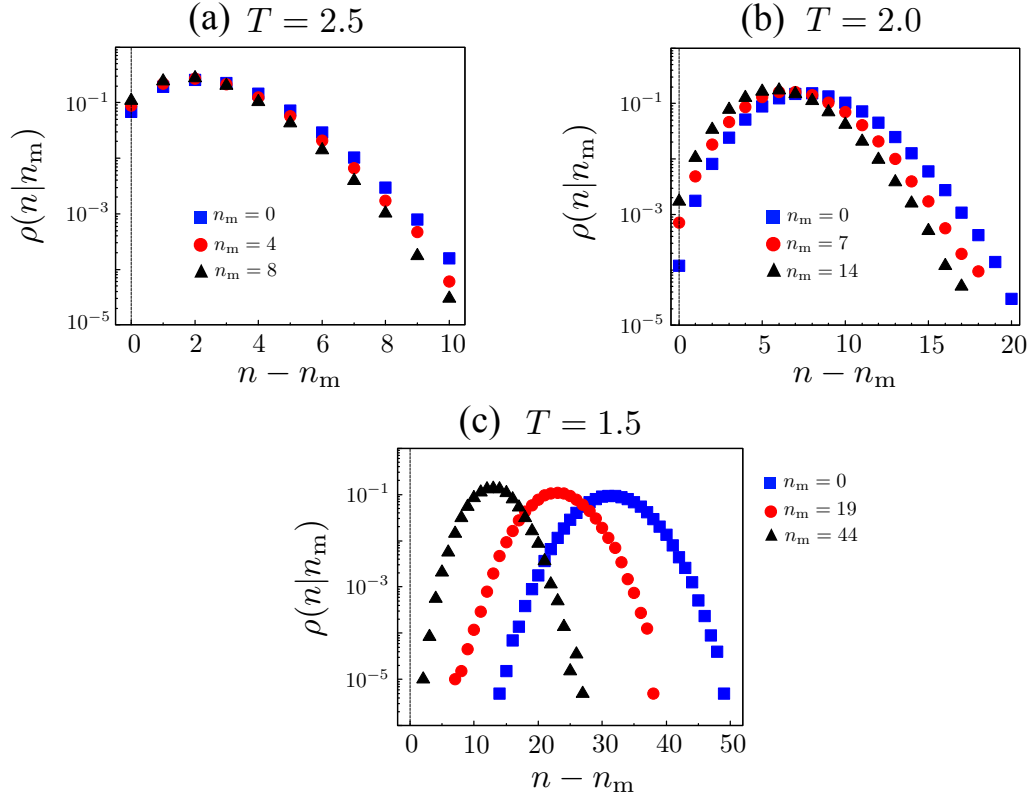


FIG. S.6. $n - n_m$ vs. $\rho(n|n_m)$ at (a) $T = 2.5$ with $n_m = 0$ (blue squares), $n_m = 3$ (red circles), and $n_m = 5$ (black triangles), (b) $T = 2.0$ with $n_m = 0$ (blue squares), $n_m = 7$ (red circles), and $n_m = 14$ (black triangles), (c) $T = 1.5$ with $n_m = 0$ (blue squares), $n_m = 19$ (red circles), and $n_m = 44$ (black triangles).

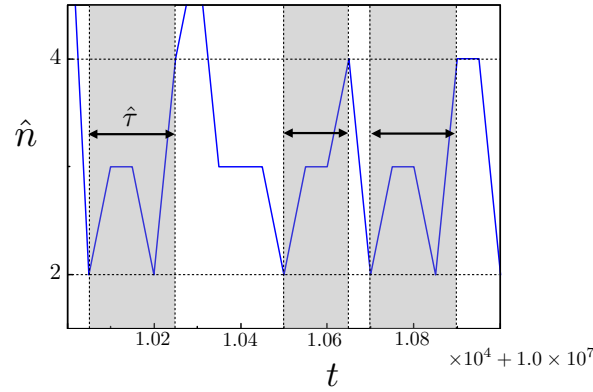


FIG. S.7. Time evolution of \hat{n} at $T = 2.5$ where $n_* \simeq 2$. Gray regions indicate waiting times, $\hat{\tau}$, from the most probable state, $\hat{n} = n_*$, to a fluctuating state with $\hat{n} = 4$.

for larger values of n_m becomes computationally demanding due to the increased number of samples required to overcome statistical fluctuations. Therefore, we chose $T = 2.5$ for this study as it provides a good balance between numerical accuracy and computational feasibility. The value of n_C should be large enough to demonstrate the effect of combinatorial enhancement, yet small enough to ensure the numerical accuracy of $\rho(n_C|0)$. From Fig. S.6(a), we find that $n_C = 10$ is an appropriate value, given our computational resources.

Figure S.7 shows a time series of \hat{n} for $T = 2.5$ and $n_C = 0$, using the criterion $r_0 = 1.5$ to identify AB_2 complexes, as determined in Supplement III. The instantaneous number \hat{n} remains small, consistent with the probability density $\rho(n|0)$ in Fig. 1 of the main text. The waiting time τ to achieve n AB_2 molecules is determined as the average first

passage time $\hat{\tau}$ from $\hat{n} = n_*$ to $\hat{n} = n$, where $n_* \simeq 2$ at $T = 2.5$. Examples of $\hat{\tau}$ for $n = 4$ are shown in Fig. S.7.

Supplement V: Explanation for Eq. (27)

We set the initial amount of C to be n and then perform a feedback protocol to bind $n' - n$ molecules from AB_2 to C when the amount of AB_2 is equal to $n' - n$. The resulting amount of molecule C is n' . Because the number of C is n' , the corresponding Hamiltonian is given by

$$H(\Gamma^{(n,n'-n)}; n') = H_C(\Gamma_A^{==}, \Gamma_A^{\neq=}, \Gamma_B^{==}, \Gamma_B^{\neq=}; n') + H_0(\Gamma_A^{\neq\neq}, \Gamma_B^{\neq\neq}) + h_{\text{int}}(\Gamma^{(n,n'-n)}) \quad (\text{V.1})$$

according to Eq. (8).

For $n = 0$, that is, without C molecules in the initial state and with n' molecules of C after the operation, the microstates are denoted as

$$\Gamma^{(0,n')} = (\Gamma_A^{\neq=}, \Gamma_A^{\neq\neq}, \Gamma_B^{\neq=}, \Gamma_B^{\neq\neq}). \quad (\text{V.2})$$

The corresponding Hamiltonian is written as

$$H(\Gamma^{(0,n')}; n') = H_C(\Gamma_A^{\neq=}, \Gamma_B^{\neq=}; n') + H_0(\Gamma_A^{\neq\neq}, \Gamma_B^{\neq\neq}) + h_{\text{int}}(\Gamma^{(0,n')}). \quad (\text{V.3})$$

which is equal to (V.1). Define the partition functions for the respective notations such that

$$Z(n') \equiv \int d\Gamma^{(0,n')} e^{-\beta H(\Gamma^{(0,n')}; n')}, \quad (\text{V.4})$$

$$Z(n, n' - n) \equiv \int d\Gamma^{(n,n'-n)} e^{-\beta H(\Gamma^{(n,n'-n)}; n')}, \quad (\text{V.5})$$

we have

$$Z(n, n' - n) = Z(n'). \quad (\text{V.6})$$

These do not indicate the distinguishability of the product history.

In contrast, the free energy is defined by taking into account the indistinguishability of molecules,

$$F(0, n') \equiv -k_B T \ln \frac{Z(n')}{(n_A - n')! n'! (n_B - 2n')! 2^{n'}}. \quad (\text{V.7})$$

$$F(n, n' - n) \equiv -k_B T \ln \frac{Z(n, n' - n)}{(n_A - n')! (n' - n)! n'! (n_B - 2n')! 2^{n'}}. \quad (\text{V.8})$$

(V.7) corresponds to $F(n')$ according to Eq. (26), while (V.8) specifies the order of the production of C molecules. Applied (V.6) to (V.8), we have Eq. (27) in the main text.

Supplement VI: Step-by-step transformation from (A3) to (A4) (to derive Eq. (21))

The path integral on the right-hand side of (A3) yields

$$\begin{aligned} & \int \mathcal{D}\hat{\Gamma}_>^\dagger \int \mathcal{D}\hat{\Gamma}_<^\dagger e^{-\beta H(\Gamma^{(n,n'-n)}(t_{\text{fin}}); n')} \mathcal{T}_{(n')}(\hat{\Gamma}_>^\dagger) \delta_{n', \hat{n}(\Gamma^{(n,n'-n)}(t_m))} \mathcal{T}_{(n)}(\hat{\Gamma}_<^\dagger) \\ &= Z(n') \int \mathcal{D}\hat{\Gamma}_<^\dagger \frac{e^{-\beta H(\Gamma^{(n,n'-n)}(t_m); n')}}{Z(n')} \delta_{n', \hat{n}(\Gamma^{(n,n'-n)}(t_m))} \mathcal{T}_{(n)}(\hat{\Gamma}_<^\dagger) \\ &= Z(n') \int d\Gamma^{(n,n'-n)} \delta_{n', \hat{n}(\Gamma^{(n,n'-n)})} \frac{e^{-\beta H(\Gamma^{(n,n'-n)}; n')}}{Z(n')} \end{aligned} \quad (\text{VI.1})$$

with $Z(n') = Z(n, n' - n)$ in (V.5). The last line of (VI.1) is not a path integral because $Z(n')$ is constant over the time interval of the path $\hat{\Gamma}_>^\dagger$, and the integrand's observable, Kronecker's delta, depends only on t_m . Combining with Eq. (10), we further transform (VI.1) as

$$= Z(n') \rho(n' | n'), \quad (\text{VI.2})$$

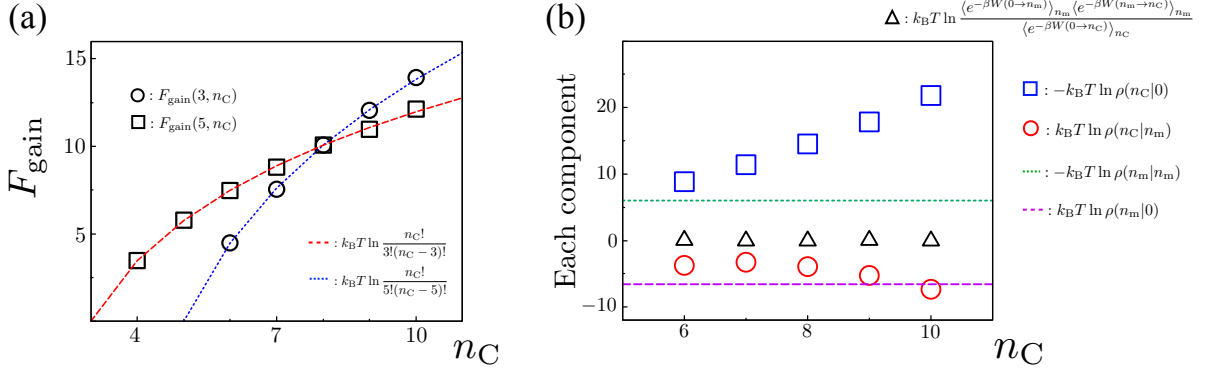


FIG. S.8. (a) F_{gain} as a function of n_C for $n_m = 3$ (circles) and $n_m = 5$ (squares) at $T = 2.5$. The dashed red line is $k_B T \ln(n_C! / (3!(n_C - 3)!))$ and the dotted blue line is $k_B T \ln(n_C! / (5!(n_C - 5)!))$. (b) Each component of (21) for $n_m = 5$ contributing to F_{gain} in (a). See text.

which is the right-hand side of (A4).

The path integral on the left-hand side of (A3) is written as

$$\int d\Gamma^{(n,n'-n)} \delta_{n',\hat{n}(\Gamma^{(n,n'-n)})} e^{-\beta W(\Gamma^{(n,n'-n)})} \times \int \mathcal{D}\hat{\Gamma}_< \int \mathcal{D}\hat{\Gamma}_> e^{-\beta H(\Gamma^{(n,n'-n)}(t_{\text{ini}});n)} \mathcal{T}_{(n)}(\hat{\Gamma}_<) \delta(\Gamma^{(n,n'-n)} - \Gamma^{(n,n'-n)}(t_m)) \mathcal{T}_{(n')}(\hat{\Gamma}_>) \quad (\text{VI.3})$$

by applying $\int d\Gamma^{(n,n'-n)} \delta(\Gamma^{(n,n'-n)} - \Gamma^{(n,n'-n)}(t_m)) = 1$. This is further transformed as

$$\begin{aligned} &= \int d\Gamma^{(n,n'-n)} \delta_{n',\hat{n}(\Gamma^{(n,n'-n)})} e^{-\beta W(\Gamma^{(n,n'-n)})} e^{-\beta H(\Gamma^{(n,n'-n)};n)} \int \mathcal{D}\hat{\Gamma}_> \delta(\Gamma^{(n,n'-n)} - \Gamma^{(n,n'-n)}(t_m)) \mathcal{T}_{(n')}(\hat{\Gamma}_>) \\ &= \int d\Gamma^{(n,n'-n)} \delta_{n',\hat{n}(\Gamma^{(n,n'-n)})} e^{-\beta W(\Gamma^{(n,n'-n)})} e^{-\beta H(\Gamma^{(n,n'-n)};n)}, \end{aligned} \quad (\text{VI.4})$$

which is the left-hand side of (A4).

Supplement VII: n_C vs. F_{gain} and contribution of each component in F_{gain}

In the main text, we demonstrated how F_{gain} depends on the number, n_m , of molecules in the intermediate state. Here, we show how F_{gain} depends on n_C , fixing n_m at 3 or 5. The numerical results, shown in Fig. S.8(a), agree well with Eq. (29) (indicated by the red and blue dotted lines). The contributions of each component to F_{gain} are displayed in Fig. S.8(b). It shows the work contribution, corresponding to the last term of Eq. (21), is negligible for any value of n_C . The functional dependence of F_{gain} on n_C arises from $-k_B T \ln \rho(n_C|0)$ and $k_B T \ln \rho(n_C|n_m)$. The former indicates the degree of rareness of the event to have n_C molecular complexes and grows almost linearly with n_C , while the latter indicates how the intermediate state reduces the waiting time.

-
- [1] John D. Weeks, David Chandler, and Hans C. Andersen, Role of Repulsive Forces in Determining the Equilibrium Structure of Simple Liquids, J. Chem. Phys. 54, 5237 (1971). DOI: 10.1063/1.1674820
 - [2] Frank H. Stillinger and Thomas A. Weber, Computer simulation of local order in condensed phases of silicon, Phys. Rev. B. 31, 5262 (1985). DOI: 10.1103/PhysRevB.31.5262
 - [3] Takenobu Nakamura, in preparation.